Contents lists available at ScienceDirect

Corrosion Science

In situ SR-XRD analysis of corrosion product formation during 'pseudo-passivation' of carbon steel in CO_2-containing aqueous environments

Joshua Owen [a],[*], Danny Burkle [a], Gaurav R. Joshi [b], Edoardo Basilico [b], Jean Kittel [b], Francois Ropital [b],[c], Sabrina Marcelin [c], Annette Kleppe [d], Richard C. Woollam [a], Richard Barker [a]

[a] Institute of Functional Surfaces, School of Mechanical Engineering, University of Leeds, Leeds LS2 9JT, United Kingdom
[b] IFP Energies Nouvelles, Etablissement de Lyon, Rond-point de l'échangeur de Solaize BP-3, Solaize 69360, France
[c] Univ. Lyon, INSA-Lyon, MATEIS UMR CNRS, Bât Blaise Pascal, 7 Avenue Jean Capelle, F-69621 Villeurbanne Cedex, France
[d] Diamond Light Source Ltd, Diamond House, Didcot, Oxfordshire OX11 0DE, United Kingdom

ARTICLE INFO

ABSTRACT

In situ Synchrotron Radiation X-ray Diffraction (SR-XRD) is employed to follow the evolution of corrosion products on X65 carbon steel in a CO_2-containing aqueous environment (80 °C, pH 6.3–7.3). A custom-designed flow cell is used to follow the real-time concomitant changes in electrochemical behaviour and corrosion product growth during stages of both natural and potentiodynamically driven 'pseudo-passivation'. We show that no deteca crystalline magnetite (Fe_3O_4) phase forms during 'pseudo-passivation' across all conditions studied. Furthermore, the results suggest the significant ennoblement observed during 'pseudo-passivation' in these experiments can be strongly related to the accumulation of iron carbonate ($FeCO_3$) on the steel surface.

1. Introduction

The dissolution of carbon dioxide (CO_2) into aqueous media creates an environment which can be highly corrosive to carbon steel, and is widely found across the energy sector (e.g. geothermal energy, carbon capture and storage) [1,2]. However, under certain conditions, a 'protective' corrosion by-product can form on the steel surface. In many instances, particularly in CO_2-saturated distilled water and sodium chloride (NaCl) brines, the reduced corrosion rate of carbon steel is attributed exclusively to the formation of iron carbonate ($FeCO_3$), formed via the following simplified reaction:

$$Fe_{(aq)}^{2+} + CO_{3(aq)}^{2-} \rightarrow FeCO_{3(s)} \qquad (1)$$

The precipitation of this crystalline layer plays a crucial role in limiting the electrochemical dissolution of the underlying steel. The formed layer is capable of reducing the corrosion kinetics by orders of magnitude as a result of the physical blocking of active sites on the steel surface and, in some instances, also acting as a diffusion barrier to electrochemically active species [3,4]. The importance of this protective corrosion product has been well recognised in the scientific literature,

being the subject of numerous investigations relating to its physical characterisation as well as the assessment and prediction of its growth and its relationship with corrosion control [5–18].

Precipitation at the steel/solution interface becomes thermodynamically favourable when the local product of iron ($a_{Fe^{2+}}$) and carbonate ($a_{CO_3^{2-}}$) ion activities exceed the solubility product (K_{sp}), or when the saturation ratio (S_{FeCO_3}) in Eq. (2) exceeds unity:

$$S_{FeCO_3} = \frac{a_{Fe^{2+}} a_{CO_3^{2-}}}{K_{sp}} \qquad (2)$$

The value of K_{sp} for $FeCO_3$ can be determined using the expression reported by Sun et al. [17], which accounts for the influence of temperature and ionic strength. Therefore, the concentration, as opposed to activity, is utilised throughout this manuscript to enable accurate calculations of S_{FeCO_3} as the ionic strength is accounted for in K_{sp} calculations.

A collection of studies examining protective corrosion product formation on carbon steel in CO_2-containing aqueous environments have reported the sudden increase in open circuit potential (OCP) during the latter stages of protective corrosion product formation [8,10,11,19].

---

* Corresponding author.
E-mail address: J.J.Owen@leeds.ac.uk (J. Owen).

This marked ennoblement in potential exceeds 100 mV in many experiments and coincides with a further reduction in corrosion rate, typically to values below 0.01 mm/year [3]. This phenomenon has been termed as 'pseudo-passivation' [20]. Furthermore, the pseudo-passivity has been shown to be reversible, since a slight decrease of pH results in a loss of protectiveness and change in OCP value [21]. A range of post-test analysis techniques have identified $FeCO_3$ as the dominant phase in environments where 'pseudo-passivation' has been reported. However, in some experiments, authors have suggested that other compounds present at the interface between $FeCO_3$ and the steel substrate are responsible for the observed 'pseudo-passivation' effect [20,22].

Han et al. [21] proposed iron hydroxide ($Fe(OH)_2$) was the compound responsible for 'pseudo-passivation' based on its potential to be thermodynamically stable under such conditions. Subsequently, a follow on study by Han et al. [20], investigated the morphology and chemical composition of the surface film formed at the interface between $FeCO_3$ and an X65 steel substrate using a series of post-test surface analytical techniques. Experiments were performed at pH 8 and 80 °C with a CO_2 partial pressure of 0.53 bar in a 1 wt% NaCl brine. Grazing incidence X-ray diffraction, transmission electron microscopy and energy dispersive X-ray spectroscopy indicated trace amounts of magnetite (Fe_3O_4) present after 'pseudo-passivation', believed to be linked to the rise in OCP. Under a comparable temperature and CO_2 partial pressure, but at pH 5.6 – 7.8, Li et al. [23] were able to show that increasing pH rapidly reduced the time associated with the onset of 'pseudo-passivation'. In contrast to the work of Han et al. [20,21], it was concluded that a 1 μm thick inner layer of $FeCO_3$ (underneath a thick outer layer of $FeCO_3$) was linked to 'pseudo-passivation'. Most recently, de Motte et al. [8] conducted a comprehensive study, using Electrochemical Impedance Spectroscopy (EIS), to follow the evolution of corrosion products on carbon steel during CO_2 corrosion. Their study showed that the rise in OCP associated with 'pseudo-passivation' is consistent with a transition to a diffusion limited process. Post-experiment cross-section analysis of the corrosion product-steel interface using electron back-scattered diffraction indicated the presence of crystalline Fe_3O_4 (10–100 nm thick) under the $FeCO_3$ layer. However, Fe_3O_4 existed as limited and isolated deposits, rather than a continuous layer, with $FeCO_3$ clearly dominating at the interface. The authors inferred that Fe_3O_4 was likely not responsible for 'pseudo-passivation' due to the dispersed nature of its presence on the steel surface and suggested the onset of diffusion impedance, due to the formation of a highly protective $FeCO_3$ layer, coincided with the increase in OCP.

Evidently, there is still a degree of ambiguity with regards to which phase and what process is responsible for 'pseudo-passivation' behaviour. However, the emergence of real-time coupling of electrochemical techniques with spectroscopic/diffraction methods have transformed the understanding of corrosion product layer growth, enabling convincing correlations to be established with electrochemical understanding and high precision analysis of the growth of surface layers [24]. This approach reduces the ambiguity in identifying the timeline of phase precipitation, preventing mischaracterisation or misinterpretation of processes because of possible changes in corrosion products induced by post-test exposure to the atmosphere. In the context of $FeCO_3$ growth in CO_2 environments, this is illustrated from the in situ work performed by Burkle et al. [19,25] in which a Synchrotron Radiation-X-ray Diffraction (SR-XRD) flow cell was used to track the nucleation and growth kinetics of $FeCO_3$ on X65 carbon steel surfaces in a CO_2-saturated NaCl solution at pH 6.3, 6.8 and 7. The growth of $FeCO_3$ on the steel surface was recorded in real time, producing transient diffraction patterns concomitantly with corrosion rate data using the linear polarisation resistance (LPR) electrochemical measurement technique. The information collected showed a clear link between $FeCO_3$ precipitation at the steel surface and the reduction in corrosion rate. 'Pseudo-passivation', however, was not observed over the short experimental period (4 h) utilised as part of that study.

In this study, following on from the findings of Burkle et al. [19,25],

the capabilities of in situ synchrotron XRD and electrochemical measurements within a flow cell configuration are exploited to observe the 'pseudo-passivation' process in real-time. By coupling in situ XRD with electrochemical methods, direct insight into the transformations of the system can be achieved at the precise time when changes occur and it can be understood how such changes manifest themselves in terms of electrochemical corrosion behaviour. In this study at 80 °C in saturated CO_2 solution conditions, the bulk solution pH range studied included pH 6.3, pH 6.8 and pH 7, as previously studied by Burkle et al. [19], and is extended to pH 7.3. The exposure period was also increased to 12 h to encourage 'pseudo-passivation' and enable mechanistic understanding of the process to be established in a CO_2-saturated environment.

2. Experimental

The following sections provide information relating to the experimental approach and the test conditions evaluated using the SR-XRD flow cell. The flow cell design is described elsewhere, which also discusses the setup, operation and full capabilities of the system [19,25]. However, a summary of the setup and operation is provided here for completeness.

2.1. SR-XRD flow cell experimental set-up

A schematic diagram of the flow cell setup at the Diamond Light Source, Oxfordshire, UK as well as an image taken in the experimental hutch itself is shown in Fig. 1. A locally heated simulated formation brine was circulated within a closed loop between the flow cell and a 1 L vessel via the use of a centrifugal micro-pump. The flow cell houses a carbon steel coupon (working electrode) from which diffraction patterns and electrochemical responses are recorded. A detailed description of the components within the system, including the platinum counter and silver/silver chloride (Ag/AgCl) reference electrode configuration is provided by Burkle et al. [25]. The setup enables in situ electrochemical measurement and SR-XRD patterns to be collected continuously from the carbon steel coupon within the flow cell during operation. Consequently, there is no interruption or change in the flow conditions during the acquisition of electrochemical data or synchrotron diffraction patterns. In each experiment, once flow was initiated through the cell, electrochemical and SR-XRD measurements commenced within 3–4 mins of the pump being switched on. This delay was predominantly due to the time taken to complete the required safety checks and evacuate the experimental hutch. Two sets of experiments were conducted at the Diamond Light Source Synchrotron facility:

i. **Anodic polarisation curves measurements**, where the 'pseudo-passivation' process was induced via stepping up the applied potential in the anodic direction away from the OCP. In these experiments we explored the influence of bulk solution pH on the propensity for 'pseudo-passivation' to occur.

ii. **A 'freely corroding' experiment**, where 'pseudo-passivation' was allowed to occur naturally in the absence of an applied potential. In this experiment the observations from diffraction patterns are cross-correlated with those obtained from the anodic polarisation curves.

2.2. Material preparation

The test coupons integrated into the flow cell were manufactured from X65 grade carbon steel, with a ferritic-pearlitic microstructure and an elemental composition (wt%) of 0.15 C, 1.42 Mn, 0.09 Ni, 0.05 Nb, 0.17 Mo, 0.22 Si, 0.06 V, 0.025 P, 0.002 S and balance Fe. Test coupons were machined into 9 mm diameter, 10 mm thick cylinders. For all experiments, the exposed X65 steel surface area in the SR-XRD cell was 0.63 cm^2. Prior to the start of each experiment, the carbon steel test coupon was wet-ground up to 600 silicon carbide grit paper, degreased with acetone, rinsed with distilled water and dried with compressed air
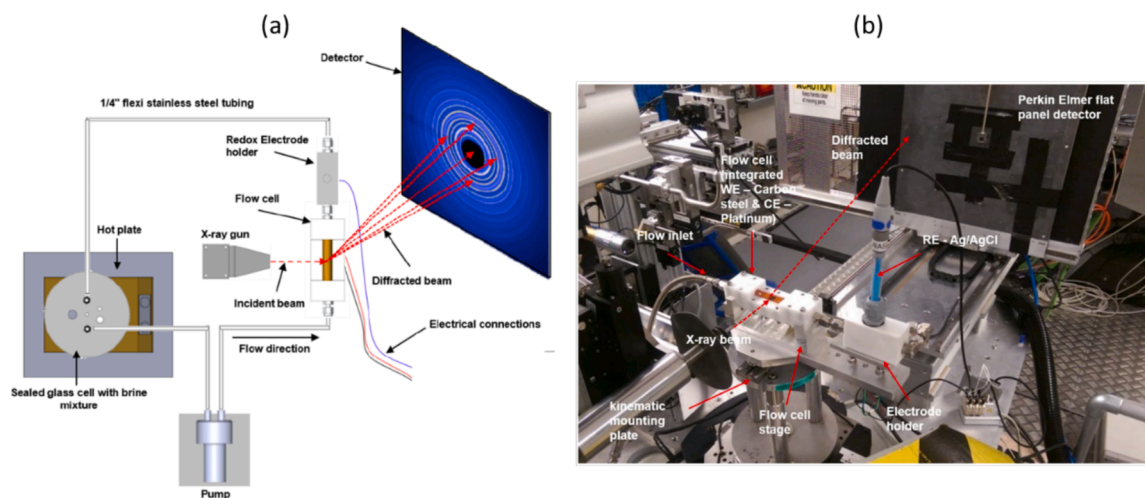
Fig. 1. (a) Schematic and (b) photograph of the flow cell set-up used on the Diamond Light Source beamline (I15).

before being immediately flush mounted into the base of the flow cell. An electrical wire was then connected to the coupon through the base of the flow cell to enable electrochemical measurements.

2.3. Solution preparation

The electrolyte was a continually bubbled CO_2-saturated 3.5 wt% NaCl solution (1 L) in an external sealed cell which was sparged with CO_2 for a minimum of 4 h prior to each experiment. The flow cell and brine vessel were all sealed with one outlet opened on the vessel lid to allow CO_2 gas to escape and prevent O_2 ingress. Indeed, it has been shown that low O_2 content in the electrolyte solution leads to localised corrosion of carbon steel [10]. Each experiment was conducted at a temperature of 80 ± 1 °C and flow velocity of 0.1 m/s. The only parameter changed between each test was the bulk solution pH, which was varied for each experiment and controlled through the addition of sodium bicarbonate ($NaHCO_3$), for pH ≤ 7 solutions, or sodium hydroxide (NaOH), for pH > 7 solution, with the aid of an automatic temperature correction pH probe. The solution pH was measured prior to the start of experiments once a temperature of 80 °C was achieved. Freely corroding experiments were performed at pH 7.3, conditions under which natural 'pseudo-passivation' would occur within an appropriate time frame for SR-XRD experiments. Potentiodynamic polarisation experiments were performed at pH 6.3, 6.8 and 7.

2.4. XRD analysis

The in situ SR-XRD experiments were conducted at beamline I15 at the Diamond Light Source, Oxfordshire. Synchrotron radiation was adjusted and focused into a monochromatic beam (70 μm in diameter) with an energy of 40 keV and wavelength of 0.30 Å. The incident-beam to coupon angle was set to 4°. To ensure accuracy and effective correlation with crystal growth, an operational loop was implemented to scan multiple measurements across the centre of each coupon. For anodic polarisation measurements, three areas were scanned across a 1 mm path length, whilst for freely corroding experiments, five areas were scanned across a 2 mm path length. A reduced scan length and area was utilised for the anodic polarisation experiments to capture the rapidly changing layer behaviour during the significantly shorter exposure period than freely corroding experiments. This information was then used to determine a cumulative intensity over the scanned regions, helping to account for any heterogeneity in growth on the steel surface. Consequently, this method of analysis enables identification of the consistency of film growth in different locations across the steel, but also provides a larger sampling size from the surface which can be more

accurately and reliably correlated with the electrochemical response. Scanning multiple areas also ensured that any local formation of other phases (such as Fe_3O_4 observed in other studies [8]) was detected. In this work, both the transient response from individual scans, as well as the average from all five scanned areas are presented to describe the non-uniform growth characteristics over the surface at OCP and to provide the most representative data possible to correlate with the collected electrochemical data. With regards to the duration of data acquisition, individual data scans at each location took 60 s to acquire an XRD pattern (including the time taken for movement to each point). Therefore, the overall scanning time to complete the five scans over a 2 mm path length was ~5 min, whilst for anodic polarisation measurements the scanning time was ~2 min. These diffraction images were recorded using a Perkin Elmer flat panel detector located 975 mm from the coupon and conventional 2θ diffraction patterns were generated by radial integration of the Debye rings using the software Fit2D with subsequent data analysis performed by profile fitting and Rietveld analysis. Damage to the surface layers, or interaction with the electrolyte initiated by the SR-XRD beam itself was not detected during this study. This was confirmed in a previous study by the authors and during repeat measurements for the purpose of *ex-situ* surface analysis (without implementing SR-XRD), which produced an equivalent evolution in the corrosion rate [19].

2.5. Electrochemical measurements

The X65 carbon steel is in active state at OCP in a pH 7.3 solution [26]. LPR measurements were performed every 5 min by applying a potential sweep to the coupon from -5 mV vs. OCP to $+5$ mV vs. OCP with a scan rate of 0.25 mV/s to obtain the polarisation resistance (R_p) and thus estimate the in situ corrosion rate as a function of time. For this experiment, the solution resistance (R_s) was measured independently in laboratory tests using Electrochemical Impedance Spectroscopy (EIS) by implementing the same three-electrode geometry and solution chemistry. The coupon was polarised at ± 5 mV vs. OCP over a frequency range from 20 kHz to 0.1 Hz, with 10 measurement points per decade. The value of R_s was determined as the high frequency limit of the real part of impedance diagram represented in Nyquist coordinates and was assumed to remain steady throughout the SR-XRD measurements. The solution resistance was deducted from the polarisation resistance obtained by LPR measurements to provide a charge-transfer resistance (R_{ct}), which was used to determine the corrosion rate (V_c) using Eq. (3). A Stern-Geary coefficient (B) of 17 mV was used in this study based on measurements in previous work under very similar operating conditions [19].

$$V_c = \frac{Ki_{corr}M_{Fe}}{n\rho F} \tag{3}$$

Where the constant K (3.16×10^8) converts the calculated corrosion into a rate expressed in mm/yr, M_{Fe} is the molar mass of iron (55.8 g/mol), n is the number of electrons involved in the anodic reaction (2), ρ is the density of iron (7.87 g/cm^3) and F is the Faraday constant (96485 C/mol). The corrosion current density, i_{corr} (mA/cm^2), is calculated from Eq. (4) and R_{ct} determined from solution resistance-corrected LPR measurements.

$$i_{corr} = \frac{B}{R_{ct}} \tag{4}$$

At a lower bulk solution pH, potentiodynamic polarisation experiments were performed by polarising from -10 mV vs OCP and scanning > 700 mV in the anodic direction at a scan rate of 0.25 mV/s to accelerate precipitation of corrosion product layers and initiate the 'pseudo-passivation' state.

2.6. Thermodynamic modelling

The open source thermodynamic model PhreeqC (Version 3.0) [27] has been used to compute the molarities and activities of the various carbonic species, H$^+$ and OH$^-$ at the different values of solution pH. This was used in conjunction with the expression for FeCO$_3$ saturation ratio and K$_{sp}$ value reported by Sun et al. [17], Eq. (5), to determine the required $c_{Fe^{2+}}$ to achieve a saturation ratio equal to 1.

$$\log K_{sp} = -59.3498 - 0.041377T_k - \frac{2.1963}{T_k} + 24.5724\log(T_k) + 2.518I^{0.5} - 0.657I \tag{5}$$

where T_k is the temperature (K) and I is the ionic strength.

2.7. Ex situ surface analysis

A selection of test coupons from the SR-XRD experiments were assessed *ex situ*. Scanning electron microscopy (SEM) was carried out in secondary electron mode at an operating voltage of 2 kV and a working distance of 4 mm, to assess coverage and topography of corrosion products. Selected coupons were prepared for cross-section analysis using a focused ion beam (FIB). The instrument used for SEM and FIB analysis was a FEI Nova200 dual beam FIB-SEM, operated at voltages between 30 kV and 2 kV, and with ion beam currents between 5 and 0.1 nA. Regions of interest were first coated with a protective layer of platinum before bulk removal of material was performed.

3. Results and discussion

3.1. Polarisation curve in the anodic domain: characterization of the pseudo-passive state

Fig. 2 shows the electrochemical response of X65 steel subjected to anodic potentiodynamic polarisation within the SR-XRD flow cell at bulk solution pH values of 6.3, 6.8 and 7. All other operating conditions remained constant for these experiments i.e., flow velocity of 0.1 m/s, temperature of 80 °C and 3.5 wt% NaCl solution, saturated with CO$_2$. The general anodic response observed in each experiment first consists of an anodic active region, where the current increases until the peak current density is reached; this is followed by a rapid decrease in current density which indicates the active-passive transition to a *relatively* protective 'pseudo-passive' state. As potential continues to increase in the passive region, the current density progressively increases until the system shifts to a trans-passive domain where the protective surface film begins to break down, resulting is a sharper rise in current with applied potential. No transpassive region was observed under pH 7 conditions.
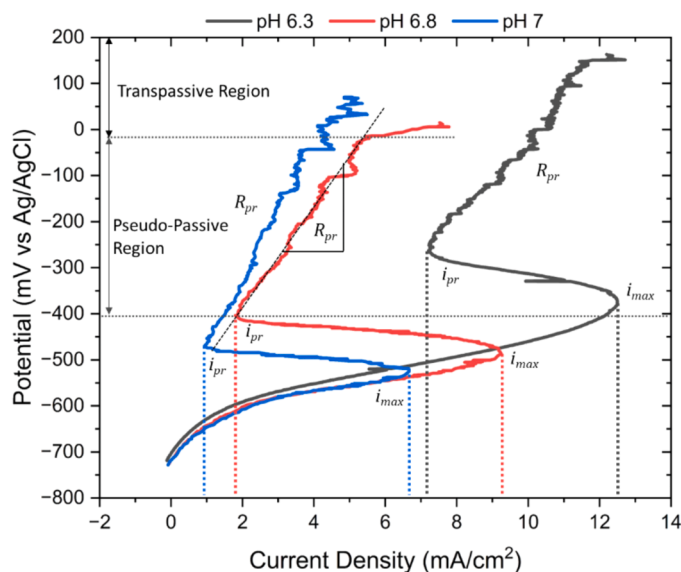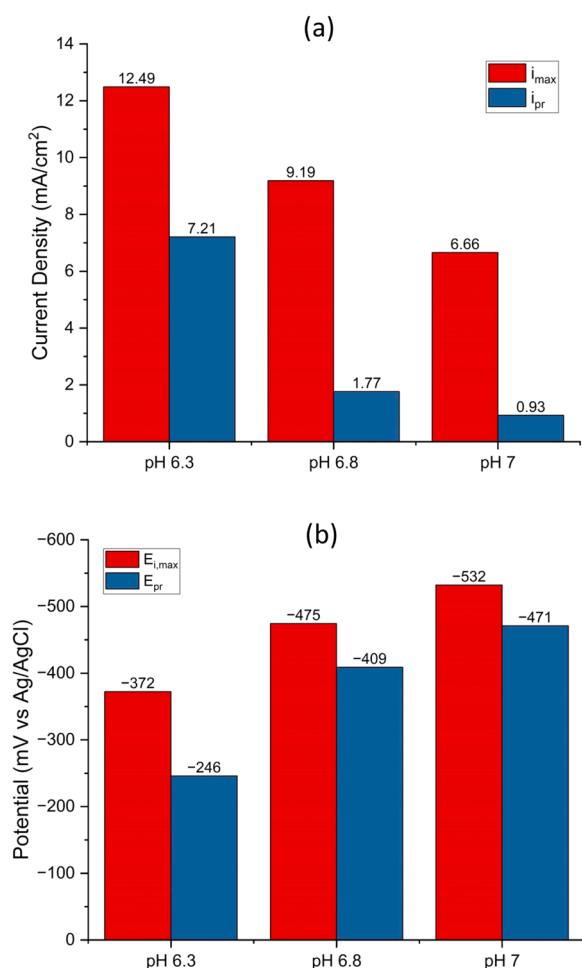

Fig. 2. Anodic polarisation curves obtained for the X65 carbon steel in a 80 $^{\circ}$C and 3.5 wt% NaCl solution saturated with CO$_2$ (0.54 bar pCO$_2$), flowing at a velocity of 0.1 m/s through the flow cell at pH 6.3, 6.8 and 7. The pseudo-passive and transpassive regions have been identified on the plot at pH 6.8. The parameter R$_{pr}$ represents the resistance observed in the passive region, as demonstrated for pH 6.8 conditions.

This observed response has been termed 'pseudo-passivation' and has been reported by numerous authors [14,20,23]. It is worth highlighting here that the 'passive' currents observed in this region are many orders of magnitude higher than that observed on corrosion resistant alloys as a result of the formation of their respective passive films [28–30].

There is a noticeable trend with regards to the polarisation response as a function of bulk solution pH. These effects are summarised in Fig. 3. As bulk pH increases, the inflection point denoting the transition from active dissolution to entering a 'passive' state is sharper and reaches a lower 'peak' current (or 'i$_{max}$', as shown in Fig. 3), prompting a more rapid transition to a protective state. The potential at which the onset of 'pseudo-passivation' occurs (E$_{pr}$) also shows a similar trend with pH, with lower E$_{pr}$ values at higher pH. Furthermore, with increasing pH, the value of i$_{max}$ indicated in Fig. 2 and Fig. 3, is reached at progressively lower potentials and 'passivation' takes place at lower current densities (denoted i$_{pr}$ in Fig. 2). The potential denoting the transition from active dissolution to a 'pseudo-passive' state is smaller, suggesting a far lower overpotential requirement to transition to a protective state as bulk solution pH increases. The anodic overpotential needed to attain i$_{max}$ (or 'E$_{i,max}$', as shown in Fig. 3) decreases from $+340$ mV vs OCP to $+235$ mV vs OCP at pH 6.3 and 6.8, respectively, and to $+205$ mV vs OCP at pH 7. Consequently, a more protective 'pseudo-passive' layer is obtained sooner at higher pH. The resistance in the 'pseudo-passivation' region (R$_{pr}$) is determined from the gradient of the data in Fig. 2 between the 'pseudo-passive' and transpassive regions, and is likely attributed to the presence of a thick layer acting as a diffusion barrier. The value of R$_{pr}$ is ~86 $\Omega \bullet$cm^2 at pH 6.3, ~102 $\Omega \bullet$cm^2 at pH 6.8 and ~123 $\Omega \bullet$cm^2 at pH 7, suggesting a more significant diffusion barrier is present as pH increases.

Fig. 4 shows the in situ SR-XRD results over the entire time span of the potentiodynamic polarisation results at pH 6.3 and pH 7 (detailed analysis was completed on the two extremities, therefore pH 6.8 analysis was omitted). The results show that FeCO$_3$ was the only crystalline phase to form at the steel surface displaying seven lattice planes of FeCO$_3$ ((104), (110), (113), (202), (204), (018) and (122)). No preferential orientation of the FeCO$_3$ was observed, but the (104) peak was most intense. The other peaks can be assigned to iron carbide (Fe$_3$C) that arise from a cementite network that remains on the surface (from the

Fig. 3. (a) Current density and (b) potential values at various stages of the 'pseudo-passivation' processes during potentiodynamic anodic polarisation of X65 carbon steel coupon in an 80°C and 3.5 wt% NaCl solution saturated with CO_2 at 0.54 bar pCO_2, flowing at a velocity of 0.1 m/s through the flow cell at pH 6.3, 6.8 and 7.

original carbon steel microstructure) as the ferrite phase preferentially corrodes [12,31]. The evolution in $FeCO_3$ crystal plane intensity over time at each of the three scanned locations is provided in Fig. 4(c). In this plot, the peak areas with respect to each plane have been normalised relative to the peak area of the Fe (110) plane. The (104) peak was the most predominant, as expected, but all peaks characteristic of $FeCO_3$ similarly increased in intensity over the experiment. These increases in intensity are interpreted to convey wide coverage of $FeCO_3$ crystallites across the X65 steel surface. The sole formation of $FeCO_3$ during the 'pseudo-passivation' stage, and the consistent trend in peak intensities, was also observed at pH 6.3.

Fig. 4(b) presents the in situ SR-XRD results over the entire time duration of the anodic potential sweep experiment during acquisition of the polarization curve at pH 7. Again, $FeCO_3$ was the main crystalline phase to form at the steel surface with seven lattice planes of $FeCO_3$ ((104), (110), (113), (202), (204), (018) and (122)) apparent. The relative intensity of these peaks compared to Fe (110) as a function of the applied anodic potential is shown in Fig. 4(d), showing a significant increase in the $FeCO_3$ (104) and (110) peaks as potential increased. Interestingly, the (021) planes of chukanovite ($Fe_2(OH)_2CO_3$) are also detected at 60 mins as the applied potential approached 0 mV vs Ag/AgCl (Fig. 2). As this phase was only observed at excessive potentials far from the point at which the system enters 'pseudo-passivation', it was not attributed to the 'pseudo-passivation' phenomena. $Fe_2(OH)_2CO_3$ has been characterised *ex-situ* in unique locations within regions of localised

corrosion on carbon steel under sand deposits in CO_2-saturated environments [32]. Ko et al. [15], Ingham et al. [33] and Sk et al. [34] have each observed $Fe_2(OH)_2CO_3$ formation alongside $FeCO_3$ in their accelerated anodic galvanostatic/in situ XRD experiments. Azoulay et al. [35] and Refait et al. [36] have shown with thermodynamic modelling, precipitation experiments and characterisation techniques (XRD, Raman and infrared spectroscopies) that $Fe_2(OH)_2CO_3$ stability over $FeCO_3$, Fe($OH)_2$ and Fe_3O_4 is favoured under high ferrous ion concentrations and relatively high bicarbonate/carbonate concentrations under high pH conditions. Remaining peaks, again, can be assigned to Fe_3C.

To further understand the electrochemical behaviour observed in the anodic domain, PhreeqC has been used to compute the molarities and activities of the various carbonic species, H^+, OH^- and the solubility product constant for $FeCO_3$ for the CO_2-saturated aqueous chemistry at pH 6.3, pH 6.8 and pH 7. These results are presented in Table 1. The thermodynamic calculations show that the solubility product constant for $FeCO_3$ increases at higher pH due to the presence of sodium bicarbonate and a resulting increase in the solution ionic strengths. Nonetheless, the concentration of Fe^{2+} needed to exceed saturation decreases by one order of magnitude from pH 6.3–6.8 and by approximately 25 times from pH 6.8 to pH 7.

Fig. 5 more clearly illustrates the concomitant change in $FeCO_3$ (and $Fe_2(OH)_2CO_3$ in terms of pH 7) growth and the current response from Tafel polarisation for the pH 6.3 and pH 7 conditions to guide the discussion on the temporally linked electrochemical/XRD observations. Fig. 5 displays the averaged integrated diffraction intensities from the most dominant peaks associated with $FeCO_3$ and $Fe_2(OH)_2CO_3$ ((104) and (012), respectively) against the measured current at the time of diffraction pattern collection. These average values represent the mean of three individually scanned locations. In each of the plots presented within Fig. 5, the intensity of $FeCO_3$ (104) peak is not detectable in the early stages of polarisation. As the current increases with applied potential and approaches the maximum peak value, there is nucleation and subsequent growth of $FeCO_3$ on the steel surface, signified by a sharp increase in the diffraction peak intensity. As the steel surface begins to enter into a pseudo-passive regime, the intensity of the (104) peak continues to increase until the 'pseudo-passive' region is fully reached. At this point, the growth of the film is slowed. At pH 7, an increase in intensity is observed at higher anodic potentials, suggesting further growth of the $FeCO_3$. This is likely explained by a significantly higher carbonate ion concentration at pH 7, reported in Table 1, promoting a higher degree of supersaturation and $FeCO_3$ precipitation.

In Fig. 5(a), a rapid increase in current density to ~12.5 mA/cm² is measured over the first 20 mins, which then decreases to ~7 mA/cm² by the 32nd minute. The increase in intensity measured by XRD commences at around 15 mins and ends around 40 mins. In Fig. 5(b), at solution pH 7, the current density increases to an i_{max} of ~7 mA/cm² with $FeCO_3$ precipitation beginning slightly earlier in the experiment (compared to pH 6.3) at around 10 mins. Extensive $FeCO_3$ nucleation across the X65 steel surface via primary heterogeneous nucleation follows over the subsequent 12–15 mins. The rate of these events at pH 7 is higher as supersaturation is more readily achieved in these conditions compared to pH 6.3 [3]. Polarising the coupon further results in an increase in dissolution rate from the steel surface, resulting in further growth of the $FeCO_3$ layer at pH 7. Finally, at pH 7, it is possible to detect the formation of $Fe_2(OH)_2CO_3$ after ~55 mins.

The simultaneous collection of in situ electrochemical data and diffraction patterns points to the fact that the 'pseudo-passive' response can be attributed to $FeCO_3$ precipitation, corroborating with the recent *ex situ* observations of de Motte et al. [8], where the presence of Fe_3O_4 was not found to be the cause of 'pseudo-passivation' of carbon steel in aqueous CO_2 environments. Considering that the formed $FeCO_3$ layers are attributable to the pseudo-passive response, the observed differences in the anodic domain as a function of pH can be expected when considering the solubility behaviour and/or nucleation and growth characteristics associated with $FeCO_3$.
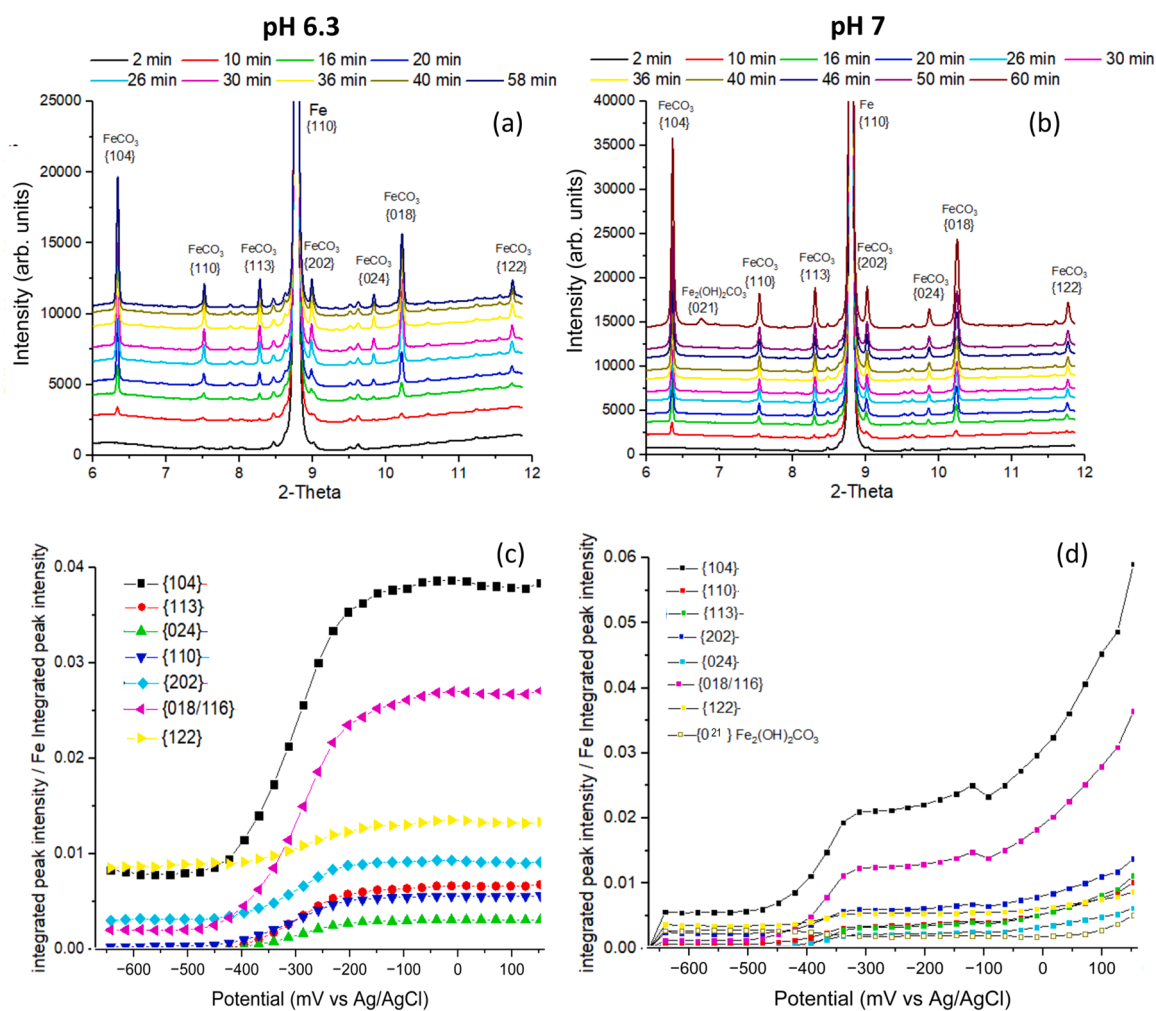
Fig. 4. *In situ* XRD analysis of an X65 carbon steel coupon in an 80 °C and 3.5 wt% NaCl saturated with CO_2 at 0.54 bar pCO_2, flowing at a velocity of 0.1 m/s through the flow cell at (a,c) pH 6.3 and (b,d) pH 7. (a,b) Individual diffraction peaks evolving with time over the course of ~1 h test duration and (c-d) the mean evolution of (104) iron carbonate peak over time intensity of the 7 lattice planes for $FeCO_3$ normalised to Fe (110) from three separate locations scanned on the steel coupon at (c) pH 6.3 and (d) pH 7. One plane from $Fe_2(OH)_2CO_3$ (021) is also included in the latter plot.

Table 1
Equilibrium concentration of species resulting from the dissociation reactions in a CO_2-H_2O system in a CO_2-saturated (0.54 bar pCO_2), 3.5 wt% NaCl solution at bulk solution pH and pH of 6.3, 6.8 and 7 and temperature of 80 °C supplemented by calculations of $FeCO_3$ solubility.

pH	$[HCO_3^-]$ (M)	$[CO_3^{2-}]$ (M)	$[H^+]$ (M)	$[OH^-]$ (M)	I (M)	$\log K_{sp}$	c_{Fe2+} (M) for $S_{FeCO_3} = 1$
6.3	1.8×10^{-2}	9.5×10^{-6}	5.0×10^{-7}	2.0×10^{-8}	0.64	-9.77	1.8×10^{-5}
6.8	5.5×10^{-2}	9.4×10^{-5}	1.6×10^{-7}	6.3×10^{-8}	0.68	-9.74	1.9×10^{-6}
7	8.5×10^{-2}	2.3×10^{-4}	1.0×10^{-7}	1.0×10^{-7}	0.72	-9.70	8.7×10^{-7}

3.2. Electrochemical behaviour at corrosion potential: "Natural" 'pseudo-passivation'

The passivation process observed when carbon steel is subjected to anodic polarisation in these experiments is attributed to the $FeCO_3$ formation. However, the 'pseudo-passive' currents observed in the scans presented in Fig. 2 are orders of magnitude greater than the corrosion current observed for a corrosion resistant alloy or a 'passivated' carbon steel reported at OCP [28–30]. Due to the excessive polarisation, this raises the question as to whether the induced passivation and that observed from 'natural' or 'self-induced' passivation results in the establishment of the same film; or at least that the same compound formation is responsible for the 'pseudo-passive' behaviour. Consequently, a final experiment was performed, in which the

'pseudo-passivation' process was allowed to occur spontaneously. To achieve this, the brine pH was increased to pH 7.3 to enable significant $FeCO_3$ formation in less than 12 h.

LPR measurement was utilised for corrosion rate determination thus enabling a direct comparison to be made with in situ XRD data. However, it is acknowledged by the authors that the accuracy of LPR measurements can diminish when $FeCO_3$ forms on a carbon steel surface [37], particularly when wider surface coverage is established and diffusion effects can influence R_p measurements, thus changing R_{ct} utilised in the corrosion rate calculation [8,11]. EIS measurements are often favoured to overcome this but require significantly longer measurements compared to the LPR technique. Therefore, as the LPR technique is widely employed for studies of $FeCO_3$ growth on carbon steel, it has been utilised in this study to demonstrate how corrosion rate
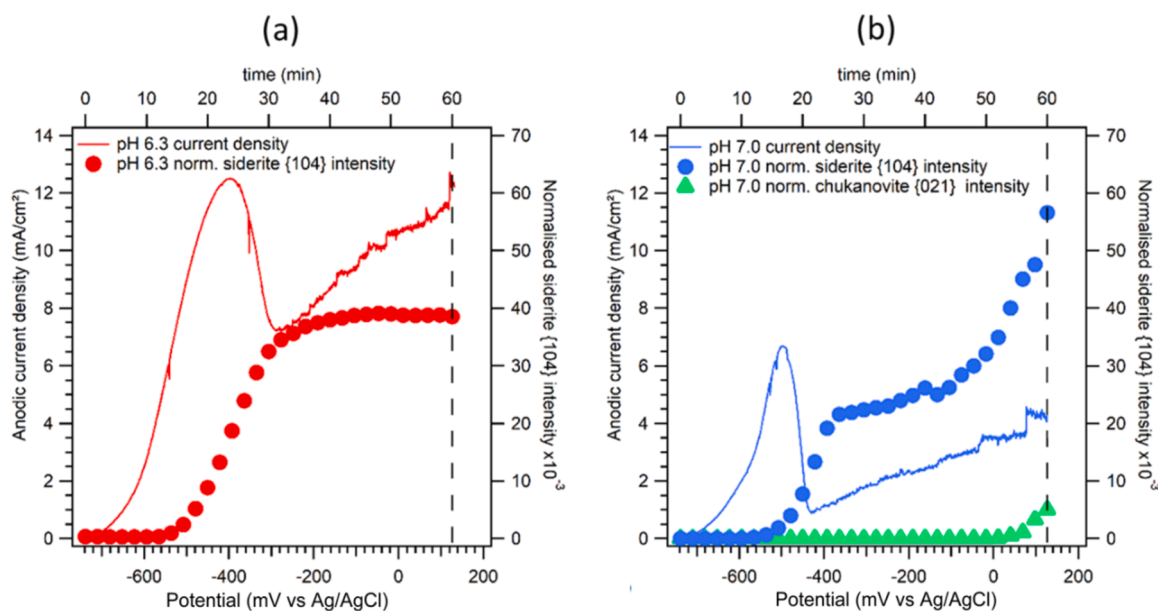
Fig. 5. Normalised $FeCO_3$ (104) and $Fe_2(OH)_2CO_3$ (021) lattice plane intensity during potentiodynamic polarisation in the anodic domain of X65 carbon steel coupon in an 80°C and 3.5 wt% NaCl solution saturated with CO_2 at 0.54 bar pCO_2, flowing at a velocity of 0.1 m/s through the flow cell at (a) pH 6.3 and (b) pH 7.

changes over the experiment duration, with the relative change in corrosion rate being of greater significance than magnitude. Fig. 6 shows the corrosion rate data and the OCP evolution from the in situ SR-XRD electrochemical test carried out in a CO_2 saturated solution at 80 °C, pH 7.3 at a flow velocity of 0.1 m/s. The OCP remains constant around −750 mV vs Ag/AgCl until 8 h of exposure time, beyond which it rises to −571 mV vs Ag/AgCl (after 9 h) and steadily to −470 mV vs Ag/AgCl (after 12 h). The corrosion rate decreases accordingly from over 1 mm/yr to approximately 0.01 mm/yr by the end of the 12 h experiment. The carbon steel is in a 'pseudo-passive' state from 7 to 8 h of exposure, which is significantly longer than that required in the presence of anodic polarisation, and a sharp decrease in the corrosion rate coincides with the onset of 'pseudo-passivation'.

Fig. 7(a) depicts diffraction patterns as a function of time, which show $FeCO_3$ was the sole corrosion product formed before and during the 'pseudo-passivation' process, with its growth being observed as corrosion rates begin to reduce. Therefore, despite the difference in

approach to achieve the 'pseudo-passivation' behaviour (polarisation vs naturally occurring), the crystalline compound associated with the process is $FeCO_3$ in both scenarios. The most intense $FeCO_3$ (104) peak at $2\theta = 6.35$ was chosen to correlate $FeCO_3$ precipitation kinetics as a function of time. Fig. 7(b) plots the $FeCO_3$ (104) peak area intensity relative to the Fe (110) substrate peak area intensity measured from five different locations across the X65 coupon as a function of time. Despite scanning multiple areas, local formation of other phases (such as $Fe_2(OH)_2CO_3$ or Fe_3O_4) were not detected in the diffractograms. The attainment of this steady state beyond 7 h is interpreted to convey a high degree of lateral coverage of a single layer of $FeCO_3$ crystallites on the X65 steel surface. 'Pseudo-passivation' occurs after 8 h of exposure time when $FeCO_3$ has already substantially precipitated abundantly on the surface. In a freely corroding environment, the precipitation of $FeCO_3$ occurs slowly and the compactness of the layer needed for 'pseudo-passivation' is reached gradually when compared against the anodic polarisation approach shown in Fig. 2.

The XRD technique detects the precipitation of film in its entirety, but it is not able to differentiate the small variations of $FeCO_3$ precipitation, such as the formation of bilayers of $FeCO_3$, that could potentially lead to enhanced corrosion protection. However, structural differences in $FeCO_3$ and/or the presence of $FeCO_3$ bilayers in protective and 'pseudo-passive' states are discerned from SEM analysis. Having identified the time periods before and after 'pseudo-passivation', two experiments were repeated under identical conditions and tests were stopped at specific time intervals, corresponding to conditions before 'pseudo-passivation' (after 6.5 h of exposure) and after 'pseudo-passivation' (after 11.5 h of exposure). The surfaces of these coupons were examined by SEM and local cross-sections were prepared and imaged using FIB-SEM, with images presented in Fig. 8.

Ex-situ SEM images of the corrosion product layer confirm that the wider protection of the surface occurs gradually. As correlated by in situ XRD analysis, abundant precipitation of corrosion product layer crystals takes place before 'pseudo-passivation'. However, the bare metal is still exposed to the solution in several areas and the thickness of the corrosion product layer is not uniform as the cross-section displays. On the contrary *ex-situ* SEM images of the corrosion product layer after 'pseudo-passivation' show an $FeCO_3$ layer that completely covers the metal underneath in the regions analysed. Some variation in crystal characteristics before and after 'pseudo-passivation' were observed, although it
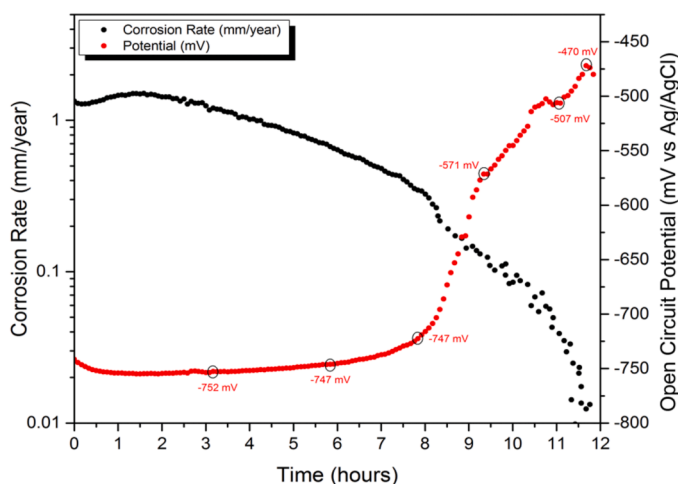

Fig. 6. OCP vs Ag/AgCl and corrosion rate, determined from LPR measurements (B = 17 mV), of a freely corroding X65 carbon steel coupon in a 80°C, pH 7.3 and 3.5 wt% NaCl solution saturated with CO_2 at 0.54 bar pCO_2, flowing at a velocity of 0.1 m/s.
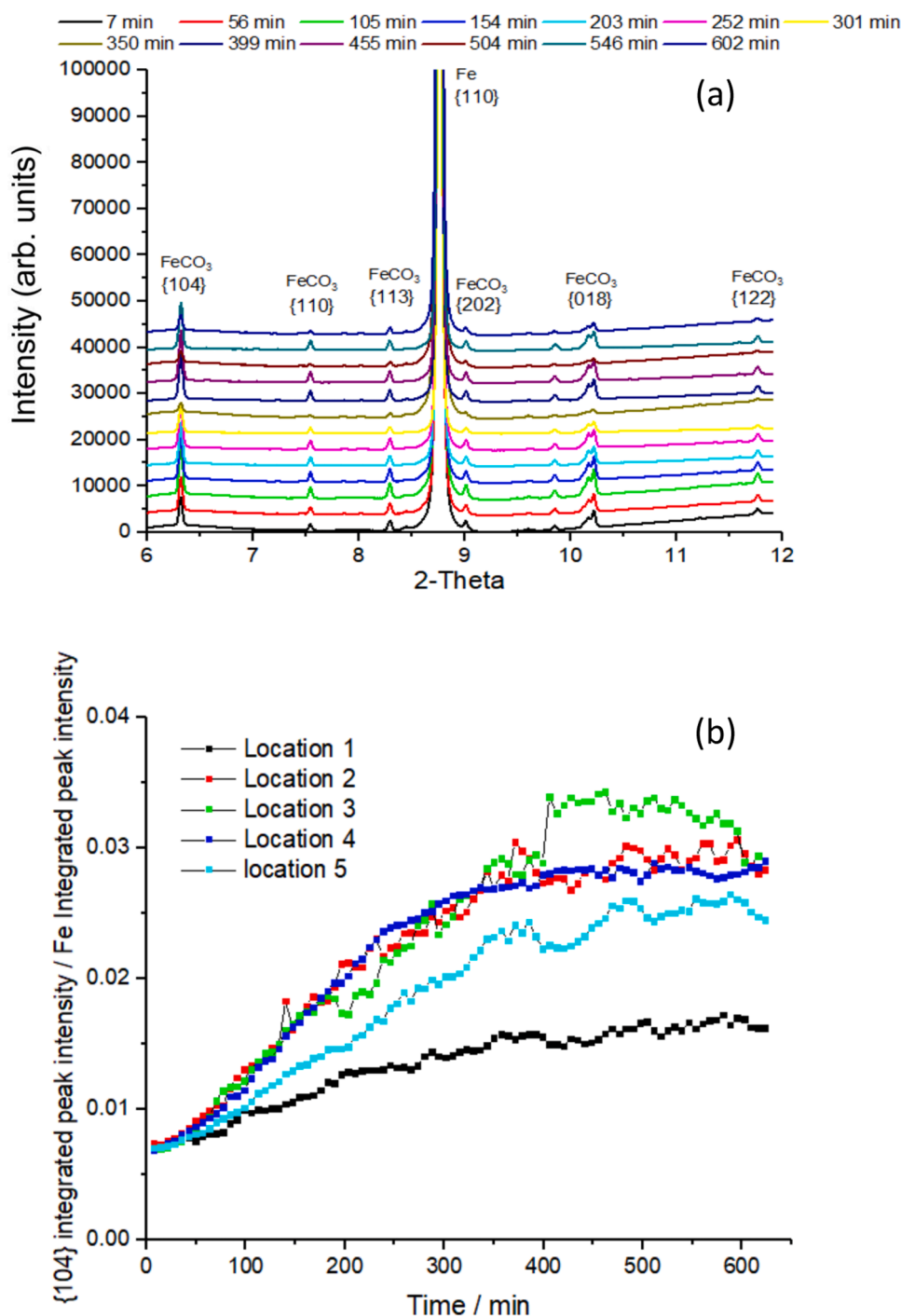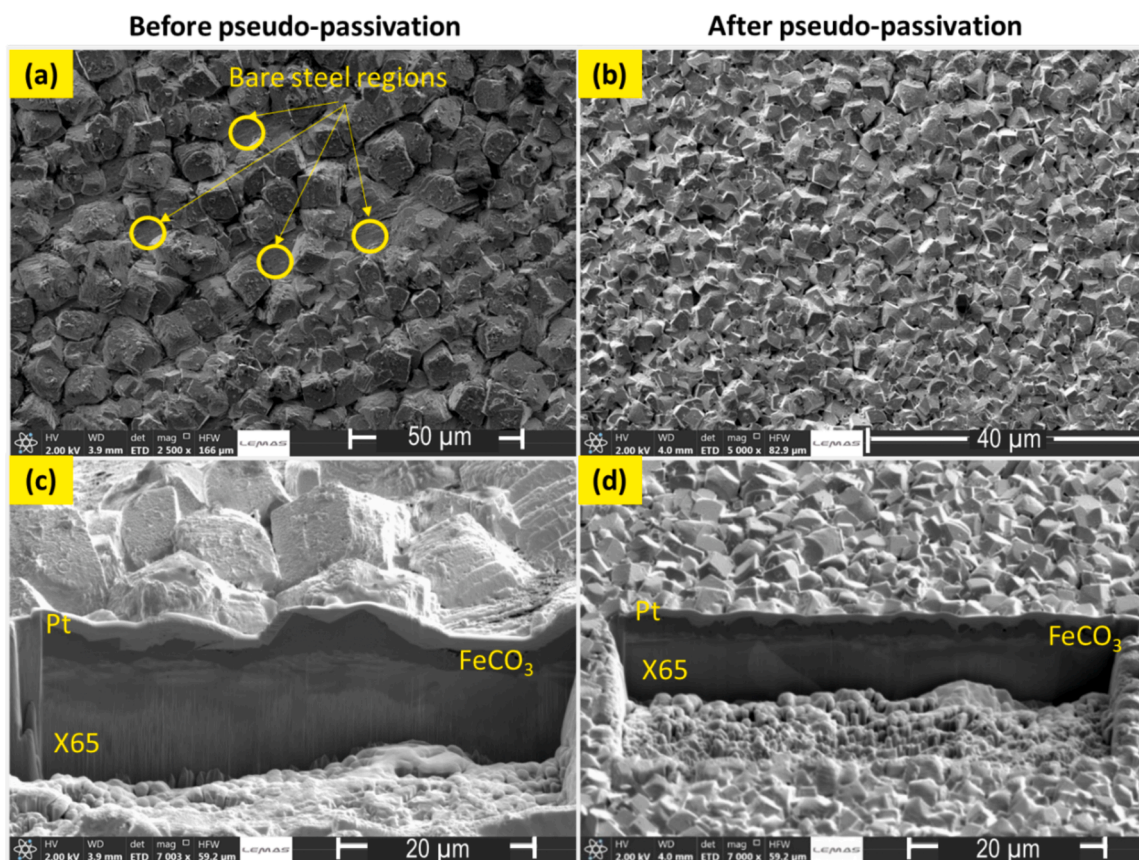
Fig. 7. *In situ* XRD analysis at OCP of an X65 carbon steel coupon in an 80 °C, pH 7.3 and 3.5 wt% NaCl solution saturated with CO_2 (0.54 bar pCO_2), flowing at a velocity of 0.1 m/s through the flow cell: (a) Individual diffraction peaks evolving with time and (b) peak intensity of the $FeCO_3$ (104) lattice planes normalized to the Fe (110) peak area, reported at five locations on the X65 carbon steel exposed surface.

should be noted that analysis was performed on specific and localised regions of the surface. However, based on the FIB-SEM analysis performed and the SR-XRD results in Fig. 7, there does appear to be a relationship in this case between the ability of the corrosion product layer to cover the surface and the protectiveness of the 'pseudo-passive' film, gradually transitioning into a diffusion barrier that interposes itself between the solution and the metal. The presence of a diffusion barrier was identified in the anodic polarisation curves in Fig. 2, corroborating with the observations in Fig. 8. De Motte et al. [8] also reported 'pseudo-passivation' behaviour in the presence of wide $FeCO_3$ surface coverage acting as a diffusion barrier, using EIS measurements to

observe significant decreases in active surface area and diffusion impedance.

FIB-SEM images also depict a layer consisting of only one major crystalline morphology in the regions analysed, and so the exclusive precipitation of an $FeCO_3$ layer appears to ensure 'pseudo-passivation' under this experimental condition. At the end of the exposure, the X65 steel coupon presents an OCP of −450 mV vs Ag/AgCl and only $FeCO_3$ is detected by SR-XRD. Thermodynamically, the most stable species at this potential/pH combination is predicted to be Fe_3O_4 [26]. *In situ* SR-XRD is sensitive to faint amounts of Fe_3O_4 [38] but it was not detected in the present study, where the dominant (311) peak would typically observed

Fig. 8. (a,b) Top-view SEM and (c,d) FIB-SEM cross-section images before (a,c) and after (b,d) 'pseudo-passivation' at OCP for the X65 carbon steel coupon in 80 °C, pH 7.3 and 3.5 wt% NaCl solution saturated with CO_2 (0.54 bar pCO_2), flowing at a velocity of 0.1 m/s through the flow cell.

between the (104) and (110) at 2θ ~7. It should be noted that SR-XRD is only able to detect crystalline species on the surface, and as a result other amorphous surface layers would be undetectable, thus requiring further study. Additionally, an $FeCO_3$ to Fe_3O_4 transformation may occur over a much longer timescale than this study, as reported by De Motte et al. [8]. However, in this study Fe_3O_4 was not responsible for the onset of 'pseudo-passivation' and the significant increase in OCP. Furthermore, the identification of Fe_3O_4 in other studies has been achieved with *ex situ* characterisation techniques, which would expose the surface layer to atmosphere and could potentially change its properties. The utilisation of in situ SR-XRD prevents environmental exposure, which may also explain why only $FeCO_3$ was detected in this study.

4. Conclusions

In situ SR-XRD has been used along with electrochemical techniques (LPR and potentiodynamic polarisation) to investigate the precipitation of the corrosion product layer during 'pseudo-passivation'. Both anodic polarisation (at a bulk solution pH of 6.3, 6.8 and 7) and at OCP (pH 7.3) were employed for investigation in a CO_2-saturated, 3.5 wt% solution, flowing through a flow cell at a temperature of 80 °C and flow velocity of 0.1 m/s. The main conclusions from the study are:

- The combination of in situ electrochemical techniques with in situ SR-XRD measurements in a bespoke flow cell enabled detailed mechanistic understanding of $FeCO_3$ formation on carbon steel and its role in 'pseudo-passivation' behaviour.
- At pH 6.3, anodic polarisation curves showed a transition from an active to a pseudo-passive state; simultaneous SR-XRD measurements indicated that $FeCO_3$ formation commenced during the active

to 'passive' transition and remains the only species (excluding substrate Fe and Fe_3C peaks) that exists on the carbon steel surface.
- Similarly at pH 7, SR-XRD measurements indicated that $FeCO_3$ was the predominant species whilst $Fe_2(OH)_2CO_3$ was detected only at high anodic potentials.
- 'Pseudo-passivation' in free corroding conditions (80 °C, pH 7.3) was observed after 8 h exposure, as a significant ennoblement of the OCP and a concurrent diminution of the LPR-determined corrosion rate. Only $FeCO_3$ layers were identified before and after 'pseudo-passivation' using SR-XRD.
- Microscopy (SEM and FIB-SEM) observations carried out on X65 coupons at different timescales (before and after 'pseudo-passivation') exposed to identical pH 7.3 conditions suggested that the X65 steel surface was not completely covered by $FeCO_3$ prior to 'pseudo-passivation'. After 'pseudo-passivation', $FeCO_3$ widely covered the surface.
- As $FeCO_3$ was observed during and after 'pseudo-passivation' under freely corroding and anodic polarisation conditions, and other layers (such as Fe_3O_4) were not detected using SR-XRD, it is suggested that the $FeCO_3$ phase plays a major role in offering the underlying steel substrate 'pseudo-passive' protection against uniform corrosion in the environment studied.

CRediT authorship contribution statement

Joshua Owen: Methodology, Formal analysis, Writing - original draft, Writing - review & editing. **Danny Burkle:** Conceptualisation, Methodology, Formal analysis, Investigation, Writing – review & editing. **Gaurav R. Joshi:** Formal analysis, Writing – review & editing. **Edoardo Basilico:** Formal analysis, Writing – review & editing. **Jean Kittel:** Formal analysis, Writing – review & editing. **Francois Ropital:**

References

[1] E. Remita, B. Tribollet, E. Sutter, V. Vivier, F. Ropital, J. Kittel, Hydrogen evolution in aqueous solutions containing dissolved CO_2: quantitative contribution of the buffering effect, Corros. Sci. 50 (5) (2008) 1433–1440.

[2] M. Kermani, A. Morshed, Carbon dioxide corrosion in oil and gas production - A compendium, CORROSION 59 (8) (2003) 659–683.

[3] R. Barker, D. Burkle, T. Charpentier, H. Thompson, A. Neville, A review of iron carbonate ($FeCO_3$) formation in the oil and gas industry, Corros. Sci. 142 (2018) 312–341.

[4] Jacklin, R., Owen, J., Burkle, D., Woollam, R.C. and Barker, R. Characterizing the Evolution of Iron Carbonate in a Demanding CO_2 Environment Using a Combined Electrochemical Impedance Spectroscopy and Linear Polarization Resistance Approach. In: AMPP Annual Conference+ Expo, Denver, CO, USA. AMPP, 2023.

[5] R. Barker, R. Yazdi, Y. Hua, A. Jackson, A. Ghanbarzadeh, M. Huggan, T. Charpentier, A. Neville, Development of an automated underwater abrasion rig to determine galvanic effects during the growth and localised breakdown of surface films in CO_2-containing solutions, Rev. Sci. Instrum. 90 (3) (2019), 034101.

[6] E. Basilico, S. Marcelin, R. Mingant, J. Kittel, M. Fregonese, F. Ropital, The effect of chemical species on the electrochemical reactions and corrosion product layer of carbon steel in CO_2 aqueous environment: a review, Mater. Corros. 72 (7) (2021) 1152–1167.

[7] R. De Motte, R. Barker, D. Burkle, S. Vargas, A. Neville, The early stages of $FeCO_3$ scale formation kinetics in CO_2 corrosion, Mater. Chem. Phys. 216 (2018) 102–111.

[8] R. De Motte, E. Basilico, R. Mingant, J. Kittel, F. Ropital, P. Combrade, S. Necib, V. Deydier, D. Crusset, S. Marcelin, A study by electrochemical impedance spectroscopy and surface analysis of corrosion product layers formed during CO_2 corrosion of low alloy steel, Corros. Sci. 172 (2020), 108666.

[9] G.R. Joshi, K. Cooper, X. Zhong, A.B. Cook, E.A. Ahmad, N.M. Harrison, D. L. Engelberg, R. Lindsay, Temporal evolution of sweet oilfield corrosion scale: phases, morphologies, habits, and protection, Corros. Sci. 142 (2018) 110–118.

[10] E. Basilico, S. Marcelin, R. Mingant, J. Kittel, M. Fregonese, R. Barker, J. Owen, A. Neville, F. Ropital, Effect of O_2 contamination on carbon steel pseudo-passive scales in CO_2 aqueous solutions, Corros. Sci. 205 (2022), 110388.

[11] A. Lazareva, J. Owen, S. Vargas, R. Barker, A. Neville, Investigation of the evolution of an iron carbonate layer and its effect on localized corrosion of X65 carbon steel in CO_2 corrosion environments, Corros. Sci. 192 (2021), 109849.

[12] Owen, J., Ropital, F., Joshi, G., Kittel, J. and Barker, R. Galvanic Interactions between Surface Layers and Bare Carbon Steel in Aqueous CO_2 Environments. In: AMPP Annual Conference + Expo, San Antonio, TX, USA. AMPP, 2022.

[13] E.V. Senatore, W. Taleb, J. Owen, Y. Hua, J.A.C.P. Gomes, R. Barker, A. Neville, Evaluation of high shear inhibitor performance in CO_2-containing flow-induced corrosion and erosion-corrosion environments in the presence and absence of iron carbonate films, Wear 404–405 (2018) 143–152.

[14] M. Gao, X. Pang, K. Gao, The growth mechanism of CO_2 corrosion product films, Corros. Sci. 53 (2) (2011) 557–568.

[15] M. Ko, B. Ingham, N. Laycock, D.E. Williams, In situ synchrotron X-ray diffraction study of the effect of microstructure and boundary layer conditions on CO_2 corrosion of pipeline steels, Corros. Sci. 90 (2015) 192–201.

[16] W. Sun, S. Nešic, Kinetics of corrosion layer formation: part 1 - iron carbonate layers in carbon dioxide corrosion, CORROSION 64 (4) (2008) 334–346.

[17] W. Sun, S. Nešić, R.C. Woollam, The effect of temperature and ionic strength on iron carbonate ($FeCO_3$) solubility limit, Corros. Sci. 51 (6) (2009) 1273–1276.

[18] J. Owen, F. Ropital, G.R. Joshi, J. Kittel, R. Barker, Galvanic effects induced by siderite and cementite surface layers on carbon steel in aqueous CO_2 environments, Corros. Sci. 209 (2022), 110762.

[19] D. Burkle, R. De Motte, W. Taleb, A. Kleppe, T. Comyn, S. Vargas, A. Neville, R. Barker, In situ SR-XRD study of $FeCO_3$ precipitation kinetics onto carbon steel in CO_2-containing environments: the influence of brine pH, Electrochim. Acta 255 (2017) 127–144.

[20] J. Han, D. Young, H. Colijn, A. Tripathi, S. Nesic, Chemistry and structure of the passive film on mild steel in CO_2 corrosion environments, Ind. Eng. Chem. Res. 48 (13) (2009) 6296–6302.

[21] J. Han, Y. Yang, S. Nesic, B.N. Brown, Roles of passivation and galvanic effects in localized CO_2 corrosion of mild steel.. CORROSION 2008, NACE International,, New Orleans, LO, 2008.

[22] Berntsen, T., Seiersten, M. and Hemmingsen, T. Effect of $FeCO_3$ supersaturation and carbide exposure on the CO_2 corrosion rate of carbon steel. In: *CORROSION 2011, Houston, TX, USA.* 2011.

[23] W. Li, B. Brown, D. Young, S. Nešić, Investigation of pseudo-passivation of mild steel in CO_2 corrosion. Corrosion 2013, NACE International,, Orlando, FL, USA, 2014, pp. 294–302.

[24] R. De Marco Z.-T. Jiang D. John M. Sercombe B.J.Ea Kinsella situ Electrochem. impedance Spectrosc. /Synchrotron Radiat. Grazing Incid. X-ray Diffr. Study Influ. acetate Carbon Dioxide Corros. mild Steel 52 11 2007 3746 3750.

[25] D. Burkle, R. De Motte, W. Taleb, A. Kleppe, T. Comyn, S. Vargas, A. Neville, R. Barker, Development of an electrochemically integrated SR-GIXRD flow cell to study $FeCO_3$ formation kinetics, Rev. Sci. Instrum. 87 (10) (2016), 105125.

[26] T. Tanupabrungsun, D. Young, B. Brown, S. Nešic, Construction and verification of pourbaix diagrams for CO_2 corrosion of mild steel valid up to 250 °C. CORROSION 2012, NACE International,, Salt Lake City, UT, USA, 2012.

[27] D.L. Parkhurst, C. Appelo, Description of input and examples for PHREEQC version 3 - a computer program for speciation, batch-reaction, one-dimensional transport, and inverse geochemical calculations, US Geol. Surv. Tech. Methods 6 (A43) (2013) 497.

[28] J. Jun, K. Holguin, G. Frankel, Pitting corrosion of very clean type 304 stainless steel, CORROSION 70 (2) (2014) 146–155.

[29] B. Ter-Ovanessian, C. Alemany-Dumont, B. Normand, Electronic and transport properties of passive films grown on different Ni-Cr binary alloys in relation to the pitting susceptibility, Electrochim. Acta 133 (2014) 373–381.

[30] Z. Zhang, B. Ter-Ovanessian, S. Marcelin, B. Normand, Investigation of the passive behavior of a Ni–Cr binary alloy using successive electrochemical impedance measurements, Electrochim. Acta 353 (2020), 136531.

[31] F. Farelas, M. Galicia, B. Brown, S. Nesic, H. Castaneda, Evolution of dissolution processes at the interface of carbon steel corroding in a CO_2 environment studied by EIS, Corros. Sci. 52 (2) (2010) 509–517.

[32] V. Pandarinathan, K. Lepková, and Van Bronswijk, W. Chukanovite ($Fe_2(OH)_2CO_3$) identified as a corrosion product at sand-deposited carbon steel in CO_2-saturated brine, Corros. Sci. 85 (2014) 26–32.

[33] B. Ingham, M. Ko, N. Laycock, N.M. Kirby, D.E. Williams, First stages of siderite crystallisation during CO_2 corrosion of steel evaluated using in situ synchrotron small-and wide-angle X-ray scattering, Faraday Discuss. 180 (2015) 171–190.

[34] M.H. Sk, A.M. Abdullah, M. Ko, B. Ingham, N. Laycock, R. Arul, D.E. Williams, Local supersaturation and the growth of protective scales during CO_2 corrosion of steel: effect of pH and solution flow, Corros. Sci. 126 (2017) 26–36.

[35] I. Azoulay, C. Rémazeilles, P. Refait, Determination of standard Gibbs free energy of formation of chukanovite and Pourbaix diagrams of iron in carbonated media, Corros. Sci. 58 (2012) 229–236.

[36] P. Refait, J. Bourdoiseau, M. Jeannin, D. Nguyen, A. Romaine, R. Sabot, Electrochemical formation of carbonated corrosion products on carbon steel in deaerated solutions, Electrochim. Acta 79 (2012) 210–217.

[37] M. Al Kindi, G.R. Joshi, K. Cooper, J. Andrews, P. Arellanes-Lozada, R. Leiva-Garcia, D.L. Engelberg, O. Bikondoa, R. Lindsay, Substrate protection with corrosion scales: can we depend on iron carbonate, ACS Appl. Mater. Interfaces 13 (48) (2021) 58193–58200.

[38] B. Ingham, M. Ko, P. Shaw, M.H. Sk, A.M. Abdullah, N. Laycock, D.E. Williams, Effects of oxygen on scale formation in CO_2 corrosion of steel in hot brine: in situ synchrotron X-ray diffraction study of anodic products, J. Electrochem. Soc. 165 (11) (2018) C756.